

# Numerical simulations of the 2D supersonic flow through the tip-section turbine blade cascade with a flat profile

J. Musil<sup>a,b,\*</sup>, J. Příhoda<sup>a</sup>, J. Fürst<sup>b</sup>

<sup>a</sup>*Institute of Thermomechanics, Czech Academy of Sciences, Dolejškova 5, 182 00 Praha 8, Czech Republic*

<sup>b</sup>*Faculty of Mechanical Engineering, Czech Technical University in Prague, Karlovo nám. 13, 121 35 Praha, Czech Republic*

Received 26 May 2020; accepted 17 August 2021

---

## Abstract

Numerical simulations of 2D compressible flow through the tip-section turbine blade cascade with a flat profile and the supersonic inlet were carried out by the OpenFOAM code using the Favre-averaged Navier-Stokes equations completed by the  $\gamma$ - $Re_{\theta t}$  bypass transition model with the SST turbulence model. Predictions completed for nominal regimes were concentrated particularly on the effect of the shock-wave/boundary layer interaction on the transition to turbulence. Further, the link between the inlet Mach number and the inlet flow angle, i.e., the so called unique incidence rule was studied. Obtained numerical results were compared with experimental data covering optical and pressure measurements.

© 2021 University of West Bohemia.

*Keywords:* supersonic tip-section blade cascade, CFD, transition modelling

---

## 1. Introduction

The compressible flow through the tip-section of turbine blade cascade of the low-pressure part of steam turbine of large output is influenced by high circumferential velocities. In the tip region the flow field is mainly supersonic, except a small subsonic region near the leading edge, see Synáč et al. [11]. Due to the supersonic inlet the inlet part of the computation domain should be modified because of the suppression of parasitic shock waves arising by the reflection from domain boundaries. Moreover a direct link between the inlet Mach number and the inlet angle exists. According to this so-called unique incidence rule (see Lakshminarayana [3]) the inlet flow angle is prescribed at the domain inlet and actual inflow parameters are determined in the distance about one chord upstream of the leading edge plane. The used blade configuration leads to considerable changes of the flow structure changes in the blade cascade at a small change of inlet flow conditions. The flow structure is affected mainly by the interaction of the exit shock wave with the shear layer on the suction side of the adjacent blade and by the interaction of the inlet shock wave upstream the blade leading edge with the shear layer on the pressure side of preceding blade, see Luxa et al. [8].

Numerical simulations of the 2D compressible flow in a turbine blade cascade with the supersonic inlet were realized for the cascade TR-U-8 representing the tip-section of the rotor blade with a flat profile. The contribution is a follow up to simulations made by Luxa et al. [6] and Straka et al. [10]. Simulations were accomplished by the RANS approach based on the Favre-averaged Navier-Stokes equations completed by the two-equation SST turbulence model and the  $\gamma$ - $Re_{\theta t}$  bypass transition model implemented in the OpenFOAM code. The particular

---

\*Corresponding author. Tel.: +420 266 053 313, e-mail: musil@it.cas.cz.  
<https://doi.org/10.24132/acm.2021.621>

aim of predictions carried out for nominal conditions was focused on the effect of the shock-wave/boundary layer interaction on the laminar/turbulent transition at various inlet free-stream turbulence intensities.

## 2. Mathematical model

Governing equations for compressible flow are based on the Favre-averaged Navier-Stokes equations completed by the two-equation SST turbulence model (Menter [9]) with the  $\gamma$ - $\text{Re}_{\theta t}$  transition model of Langtry and Menter [4]. The turbulent heat transfer is modelled by the simple assumption of the constant turbulent Prandtl number. The bypass transition model includes two transport equations. The intermittency coefficient  $\gamma$  is given by the equation

$$\frac{\partial(\rho\gamma)}{\partial t} + \frac{\partial(\rho U_j \gamma)}{\partial x_j} = P_\gamma - E_\gamma + \frac{\partial}{\partial x_j} \left[ \left( \mu + \frac{\mu_t}{\sigma_\gamma} \right) \frac{\partial \gamma}{\partial x_j} \right]. \quad (1)$$

The production term

$$P_\gamma = F_{\text{length}} C_{a1} \rho S (\gamma F_{\text{onset}})^{1/2} (1 - C_{e1} \gamma) \quad (2)$$

contains empirical correlations  $F_{\text{onset}}$  for the transition onset and  $F_{\text{length}}$  for the transition length. The destruction term

$$E_\gamma = C_{a2} \rho \Omega \gamma F_{\text{turb}} (C_{e2} \gamma - 1) \quad (3)$$

allows to simulate the relaminarization of the boundary layer. The parameter  $S = (2S_{ij}S_{ij})^{1/2}$  is the strain rate magnitude and  $\Omega = (2\Omega_{ij}\Omega_{ij})^{1/2}$  is the vorticity magnitude. The local Reynolds number  $\widetilde{\text{Re}}_{\theta t}$  for the transition onset is given by the transport equation

$$\frac{\partial(\rho\widetilde{\text{Re}}_{\theta t})}{\partial t} + \frac{\partial(\rho U_j \widetilde{\text{Re}}_{\theta t})}{\partial x_j} = P_{\theta t} + \frac{\partial}{\partial x_j} \left[ \sigma_{\theta t} (\mu + \mu_t) \frac{\partial \widetilde{\text{Re}}_{\theta t}}{\partial x_j} \right]. \quad (4)$$

The local Reynolds number  $\widetilde{\text{Re}}_{\theta t}$  is used for the determination of the onset of transition given by the critical Reynolds number  $\text{Re}_{\theta c}$  and the length of the transition region  $L_{\text{length}}$ . The application of local variables is enabled by the relation  $\text{Re}_\theta = \text{Re}_{\nu \max} / 2.193$  where  $\text{Re}_{\nu \max}$  is the maximum of the vorticity Reynolds number  $\text{Re}_\nu = y^2 |\Omega| / \nu$ . This relation is valid for the Blasius boundary layer only.

The transition model is switched to a simple algebraic transition in the case of the transition in separated flow. The intermittency coefficient is determined from the equation

$$\gamma_{\text{sep}} = \min \left[ s_1 \max \left( 0, \frac{\text{Re}_\nu}{3.235 \text{Re}_{\theta c}} - 1 \right) F_{\text{reattach}}, 2 \right] F_{\theta t} \quad (5)$$

with the dumping function

$$F_{\text{reattach}} = \exp \left[ -(R_T/20)^4 \right]. \quad (6)$$

The effective intermittency coefficient is prescribed by the relation

$$\gamma_{\text{eff}} = \max(\gamma, \gamma_{\text{sep}}). \quad (7)$$

The used empirical correlations were published for the first time by Langtry and Menter [4].

The SST turbulence model is used for the estimation of turbulent scales given by the turbulent energy  $k$  and the specific dissipation rate  $\omega$  in the form

$$\frac{\partial(\rho k)}{\partial t} + \frac{\partial(\rho \bar{U}_j k)}{\partial x_j} = \tilde{P}_k - \tilde{D}_k + \frac{\partial}{\partial x_j} \left[ (\mu + \sigma_k \mu_t) \frac{\partial k}{\partial x_j} \right], \quad (8)$$

$$\frac{\partial(\rho \omega)}{\partial t} + \frac{\partial(\rho \bar{U}_j \omega)}{\partial x_j} = \alpha \frac{P_k}{\nu_t} - \beta \rho \omega^2 + \frac{\partial}{\partial x_j} \left[ (\mu + \sigma_\omega \mu_t) \frac{\partial \omega}{\partial x_j} \right] + (1 - F_1) 2 \rho \sigma_{\omega 2} \frac{1}{\omega} \frac{\partial k}{\partial x_j} \frac{\partial \omega}{\partial x_j}, \quad (9)$$

$$\tilde{P}_k = \gamma_{eff} P_k, \quad (10)$$

$$\tilde{D}_k = \min[\max(\gamma_{eff}, 0.1), 1] D_k, \quad (11)$$

where  $P_k$  and  $D_k$  are the production and destruction terms in the original turbulence model. The  $\omega$  equation is switched over to the  $\varepsilon$  equation in the free-stream region.

Simulations were carried out by means of the open-source software OpenFOAM using the LU-SGS solver for turbulent compressible flows implemented into the code. The solver developed by Fürst [2] is based on the first order implicit scheme in time, second order linear upwind scheme for convection and second order linear scheme for viscous fluxes.

### 3. Results

The blade cascade TR-U-8 was designed for two nominal regimes given by the inlet Mach number  $M_1 = 1.2$  and isentropic outlet Mach numbers  $M_{2is} = 1.7$  and  $1.9$ . The isentropic outlet Reynolds number was  $Re_c \approx 2 \times 10^6$ . The blade cascade is formed by practically linear profiles with cambered parts near the leading and trailing edge. Main blade cascade parameters are the chord  $c = 150$  mm, the relative spacing  $s/c = 0.904$  and the stagger angle  $\gamma = 81.6^\circ$ . The chord is determined by the length measured along the linear part of the lower side of the blade profile. The axial blade chord is  $b/c = 0.162$ . Pressure and suction sides are on the inverse blade sides than usually due to the stagger angle and inlet boundary conditions.

Numerical simulations of 2D compressible flow through the blade cascade were carried out at free-stream turbulence  $Tu = 1.5\%$  with the isentropic outlet Mach numbers  $M_{2is} = 1.734, 1.909$  and  $2.011$ . Further simulations were accomplished for different inlet free-stream turbulence. Simulations were compared with experimental data of Luxa and Šimurda [7] covering optical and pressure measurements. The data reduction method proposed by Amecke and Šafařík [1] was used for the evaluation of numerical results.

The setting-up of inlet flow conditions for the supersonic inlet in numerical simulations is difficult due to the unique incidence rule expressing the link between the inlet Mach number and the inlet flow angle. In some extent the inlet Mach number is very sensitive to small changes of the inlet angle  $\alpha_1$  following by substantial changes of the flow field structure upstream of the blade cascade.

The computation domain includes the spacing of the blade cascade and is extended to  $2.37t$  upstream of the blade cascade due to the elimination of parasitic shock waves arising by their reflection from domain boundaries. The outlet part of the domain is likewise shifted downstream of trailing edges. The sketch of the computational domain is given in Fig. 1. The computational grid contains about 180 000 cells of mostly tetrahedron shape in free stream and rectangular shape in shear layers near the blade. The 2D calculation with 40 000 iterations takes on the computer with 32 cores about 3 hours. The residual of the momentum equation is assumed to be satisfied for values lower than  $5 \times 10^{-6}$ . The distance of the nearest node from the wall is  $n^+ \approx 1$ . The detail of the mesh in the vicinity of blades is given in Fig. 2.

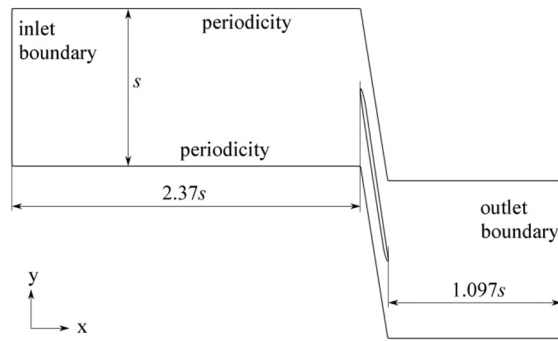


Fig. 1. Sketch of the computation domain

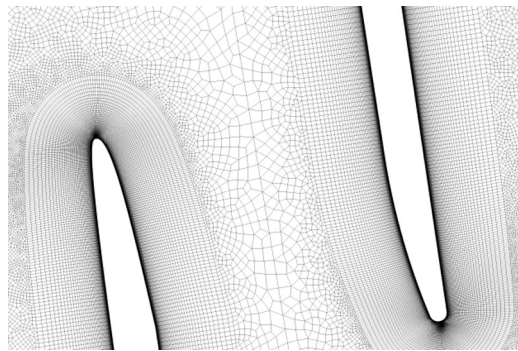


Fig. 2. Detail of the computational grid

The constant total pressure, total temperature and inlet flow angle are used as inlet boundary conditions. As the non-reflecting condition the mean static pressure determined from the outlet isentropic Mach number  $M_{2is}$  is applied as the outlet boundary condition. Further the condition  $\partial T/\partial n = \partial k/\partial n = \partial \omega/\partial n = 0$  is used. Periodic boundary conditions are utilized on both side boundaries of the computation domain. The inlet free-stream turbulence was chosen in order to obtain the value  $Tu = 1.5\%$  about one pitch upstream of the leading edge plane. The dependence of the inlet Mach number  $M_1$  on the inlet angle  $\alpha_1$  was in detail studied and is shown in Fig. 3. According to Fig. 3, the inlet angle  $\alpha_1 = 82.82^\circ$  and the inlet Mach number  $M_1 = 1.135$  were used in presented numerical results.

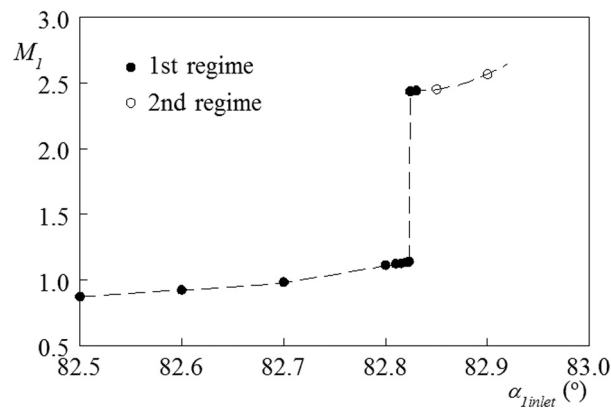


Fig. 3. Variation of the inlet Mach number with the inlet flow angle

Results for the nominal regime with the isentropic outlet Mach number  $M_{2is} = 1.734$  are further presented. Interferometric and schlieren pictures given in Fig. 4 are used for the comparison of flow fields in the blade cascade. The distribution of the isentropic Mach number on the blade is compared with numerical simulation in Fig. 5.



Fig. 4. Interferometric and schlieren pictures

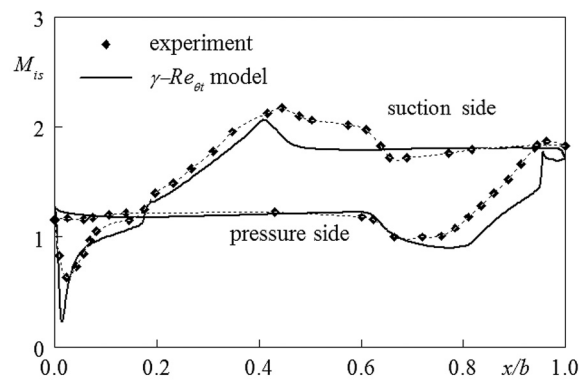


Fig. 5. Distribution of the isentropic Mach number

As follows from experimental results the flow in the blade cascade is practically supersonic except a small area near the leading edge. The flow structure is influenced mainly by interactions of shock waves with shear layer. The transition in attached flow on the pressure side downstream of the leading edge is a result of the interaction with the inner branch of the inlet shock wave. The greatest impact on the flow structure has the interaction of the inner branch of the exit shock wave of the adjacent blade with the boundary layer on the suction side where the transition in separated flow occurs at the distance  $x/b \approx 0.45$ . The flow is further influenced by the change of the curved inlet part to the straight part of the blade at  $x/b \approx 0.2$  with an abrupt change of the surface curvature.

Further, a reflected shock wave can be seen in interferometric and schlieren pictures. Therefore a perforated tailboard situated downstream the side blade is used for the suppression of such reflections in some measurements. This configuration leads on one hand to more accurate estimation of energy losses behind the cascade but on other hand to increasing of the isentropic outlet Mach number and the different angle of the exit shock wave. The flow structure in the inter-blade channel is then somewhat changed. This is the reason why the numerical simulations were compared with measurements without the tailboard.

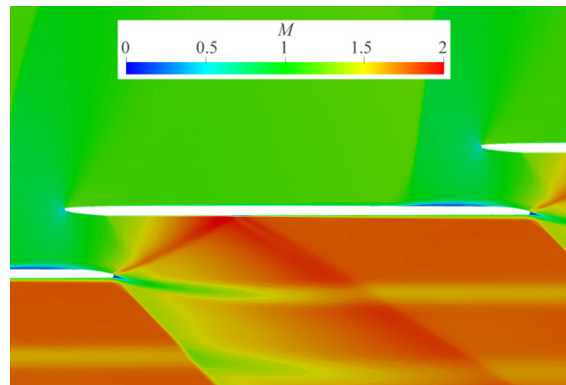


Fig. 6. Field of Mach number isolines

The Mach number isolines obtained by numerical simulation are shown in Fig. 6. The flow structure is similar to the interferometric picture. It follows from the distribution of the isentropic Mach number that rather lower values of the Mach number occur downstream the leading edge on the suction side due to differences in the adjustment of inlet boundary conditions. The position of the impact of the exit shock wave on the suction side is about  $x/b = 0.4$  in numerical simulation. The agreement of the simulation with experiment is quite acceptable. Differences can be seen only downstream the interaction with the exit shock wave on the suction side and after the velocity decrease on the pressure side.

Details of the flow field near the trailing edge are shown in Fig. 7. Flow separation arises on both blade sides upstream the trailing edge due to the used geometrical configuration leads to flow separation. The supersonic expansion near the pressure side upstream of the asymmetric trailing edge is obvious from the both results. The near wake is shifted in the suction side direction and the inlet part of exit shock wave is very thick. Therefore a considerable supersonic deviation of the flow takes place downstream the trailing edge.

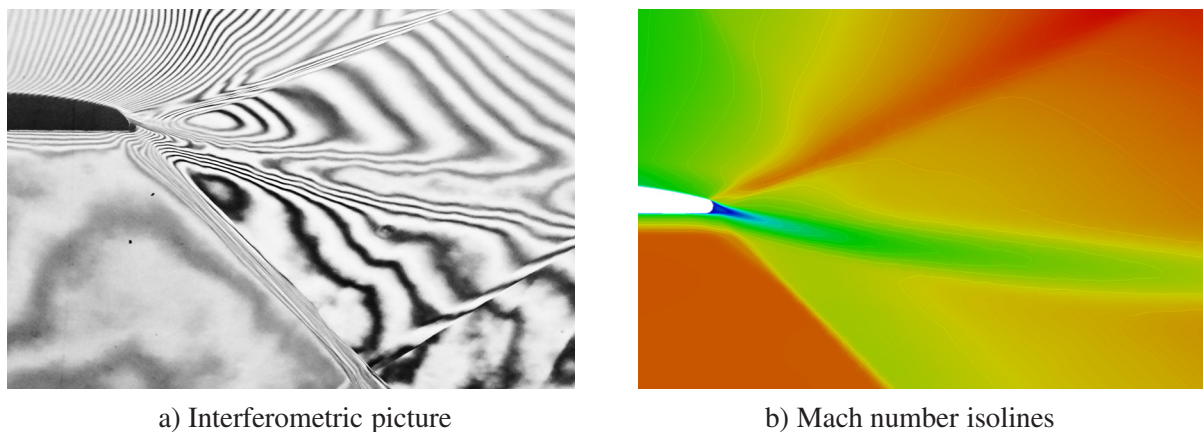


Fig. 7. Supersonic flow field in the trailing edge area

The flow structure in the blade cascade is as well expressed by the distribution of the skin friction coefficient in Fig. 8. The skin friction coefficient is expressed by means of the inlet dynamic pressure  $p_{d1}$  in the form  $C_f = \tau_w/p_{d1}$ . The application of the transition model is shown in Fig. 8a. The transition in attached flow on the pressure side comes up near downstream of the leading edge. Further, a slow decrease of  $C_f$  continues up to the interaction of the shock wave with the turbulent boundary layer at  $x/b \approx 0.65$ . The interaction with the laminar boundary

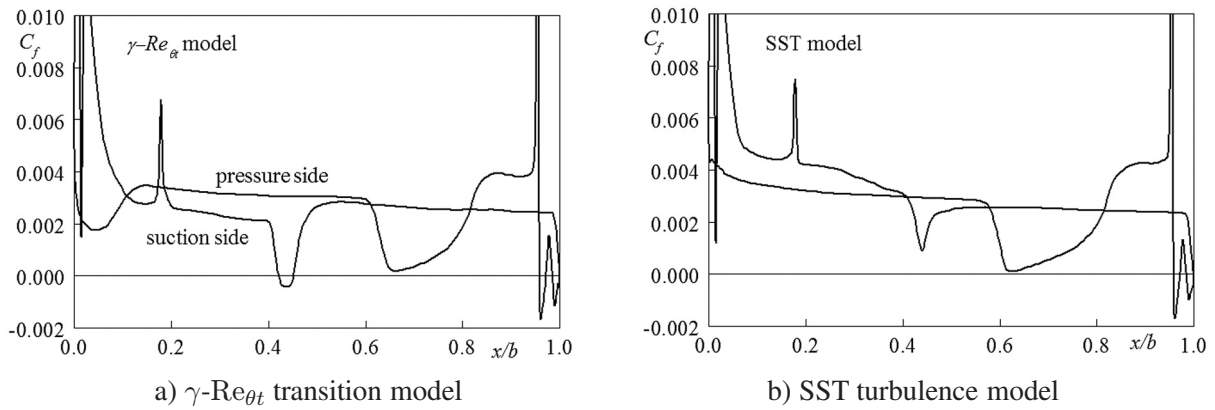


Fig. 8. Distribution of the skin friction coefficient

layer on the suction side results in the transition in separated flow. The extent of the separation on the suction side is about  $\Delta(x/b)_{sep} = (0.422; 0.452)$ . The impact of the shock wave moves downstream with the increasing Mach number  $M_{2is}$ . The skin friction coefficient obtained by the SST turbulence model is shown in Fig. 8b for comparison. Values of  $C_f$  are higher without the transition downstream the leading edge on the pressure side and without separation at the interaction with the shock wave on the suction side. The loss coefficient is only slightly higher for the SST turbulence model due to higher friction losses.

The effect of the isentropic outlet Mach number and the free-stream turbulence on the position of the separation is shown in Fig. 9. The extent of separation in experiments was estimated from interferometric pictures. The impact of the exit shock wave on the suction side moves naturally downstream with the increasing outlet Mach number  $M_{2is}$ . The shift of the separation zone is somewhat faster in case of numerical simulations due to the supersonic inlet with different adjustment of inlet boundary condition in comparison with experiment. Nevertheless, the agreement of numerical simulations with experimental data is acceptable.

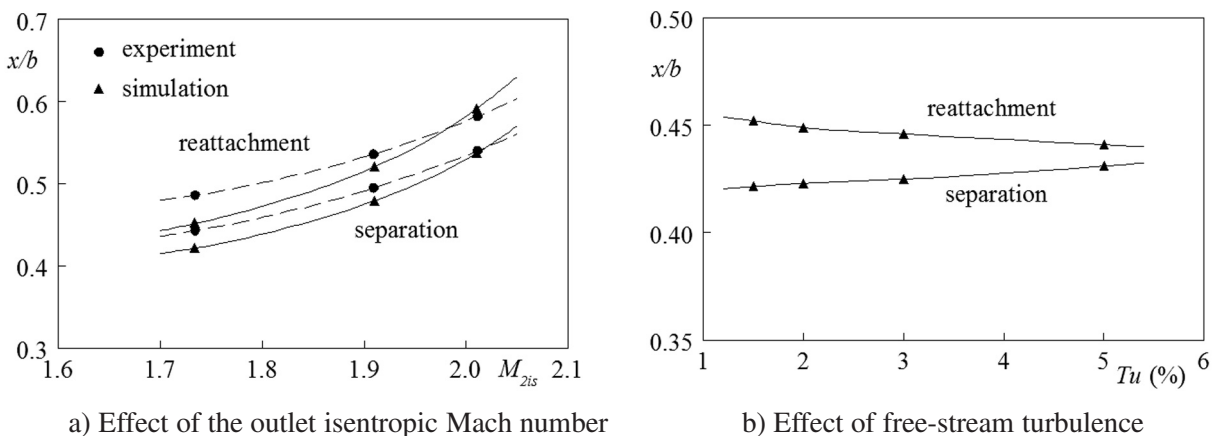


Fig. 9. Extent of the separation region

The interaction with the laminar boundary layer and the flow separation can be prevented by high free-stream turbulence and/or by a rough strip on the suction side downstream of the leading edge, e.g., see Schwaba et al. [12]. Numerical simulations were carried for various inlet free-stream turbulence and the isentropic outlet Mach number  $M_{2is} = 1.734$ . As can be seen

in Fig. 9b, the extent of the separation is decreasing with the growth of free-stream turbulence. The transition to turbulence at  $Tu = 8\%$  occurs just downstream the leading edge and the shock-wave/boundary-layer interaction on the suction side is without separation.

The mean flow parameters were determined in the traversing plane behind the blade cascade using the data reduction method. The energy loss coefficient is given by the relation

$$\zeta = 1 - (w_2/w_{2is})^2, \tag{12}$$

where  $w_2$  is the mean velocity in the traversing plane and  $w_{2is}$  is the isentropic outlet velocity estimated by means of the data reduction method. Values of the loss coefficient and the outlet flow angle are related to experimental data for the nominal regime. The variation of the both parameters with the isentropic outlet Mach number is shown in Fig. 10.

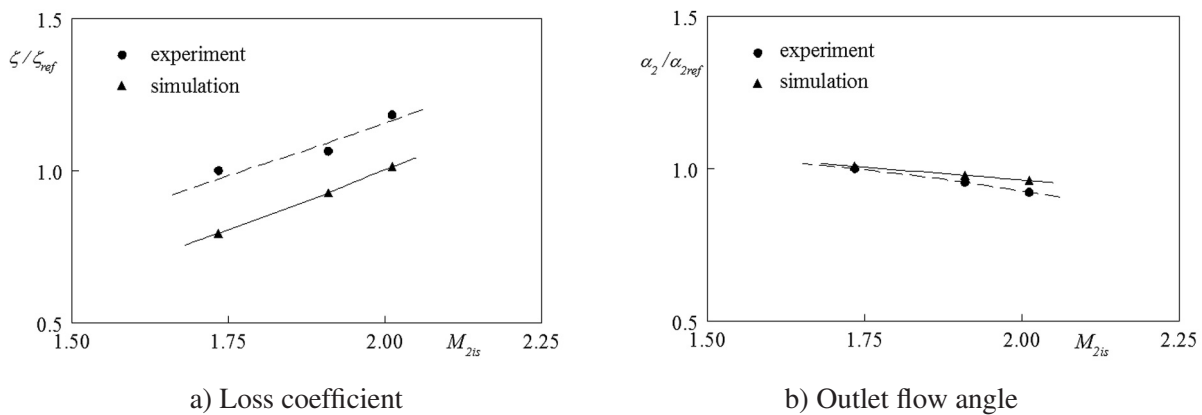


Fig. 10. Variation of the loss coefficient and the outlet flow angle with the isentropic outlet Mach number

The dependence of the calculated loss coefficient on the Mach number is same as for experimental data but calculated values are by 20% smaller than experimental results. The agreement of outlet flow angles is quite satisfactory.

As it was mentioned the flow in the inter-blade channel is influenced by shock waves reflected from side walls of the test section. Therefore numerical results give lower values of the loss coefficient but the reliable outlet flow angle.

The comparison with experimental results obtained with the perforated tailboard should give on the contrary more reliable energy losses but changes of the outlet flow angle due to some changes of the flow structure. More reliable numerical results can be achieved using the computational domain corresponding to the arrangement of the wind-tunnel test section including the following settling chamber, see Louda and Příhoda [5]. Some improvement can be achieved partly by the quasi-3D simulation and partly by the application of the URANS approach as the boundary-layer/shock-wave interaction is in some measure non-stationary.

#### 4. Conclusion

Numerical simulations of 2D compressible flow through the tip-section turbine blade cascade with the supersonic inlet were accomplished for various boundary conditions. Simulations were realized by the  $\gamma$ - $Re_{\theta t}$  transition model with the SST turbulence model implemented in the OpenFOAM code. The attention was given partly to the effect of the shock-wave/boundary-layer interaction on the transition to turbulence and partly to the adjustment of corresponding inlet conditions.

The interaction of the shock wave with the laminar boundary layer on the suction side results in the separation-induced transition with noticeable changes in the flow structure in the inter-blade channel. The effect of free-stream turbulence on this interaction is not too apparent. Due to the supersonic inlet the relation between the inlet Mach number and the inlet flow angle upstream the cascade was in detail studied.

Numerical results were compared with optical and pressure experimental data. The agreement of numerical results with experiment is acceptable. A better agreement is limited by the complicate boundary conditions given partly by the fixed link between the inlet Mach number and the inlet flow angle and partly by the effect of the shock wave reflected from the side wall of the test section.

### **Acknowledgements**

The work was supported partly by grant TH02020057 of the Technology Agency of the Czech Republic and the project SGS19/154/OHK2/3T/12 and partly by the institutional support RVO 61388998.

### **References**

- [1] Amecke, J., Šafařík, P., Date reduction of wake flow measurements with injection of another gas, DLR-Forschungsbericht 95–32, Göttingen, 1995.
- [2] Fürst, J., Development of a coupled matrix-free LU-SGS solver for turbulent compressible flows, *Computers & Fluids* 172 (2018) 332–339. <https://doi.org/10.1016/j.compfluid.2018.04.020>
- [3] Lakshminarayana, B., Fluid dynamics and heat transfer of turbomachinery, Wiley Interscience Publication, New York, 1996. <https://doi.org/10.1002/9780470172629>
- [4] Langtry, R.B., Menter, F.R., Correlation-based transition modeling for unstructured parallelized computational fluid dynamics codes, *AIAA Journal* 47 (12) (2009) 2894–2906. <https://doi.org/10.2514/1.42362>
- [5] Louda, P., Příhoda, J., Numerical modelling of transonic flows in wind tunnel test section, Proceedings of the 17th International Conference on Fluid Flow Technologies Conference on Modelling Fluid Flow (CMFF18), Budapest, 2018.
- [6] Luxa, M., Příhoda, J., Šimurda, D., Straka, P., Synáč, J., Investigation of the compressible flow through the tip-section turbine blade cascade with supersonic inlet, *Journal of Thermal Science* 25 (2016) 138–144. <https://doi.org/10.1007/s11630-016-0844-0>
- [7] Luxa, M., Šimurda, D., Optical and pneumatic measurements on TR-U-8 cascade, Czech Academy of Sciences, Institute of Thermomechanics, Research Report Z-1558/18, 2018.
- [8] Luxa, M., Šimurda, D., Příhoda, J., Váchová, J., Shock wave – boundary layer interaction in profile cascades representing rotor blading of the last stage of large output steam turbines, Proceedings of the 7th European Congress on Computational Methods in Applied Sciences and Engineering (ECCOMAS), 2016, pp. 1464–1473. <https://doi.org/10.7712/100016.1900.11964>
- [9] Menter, F.R., Two-equation eddy-viscosity turbulence models for engineering applications, *AIAA Journal* 32 (8) (1994) 1598–1605. <https://doi.org/10.2514/3.12149>
- [10] Straka, P., Příhoda, J., Fenderl, D., Rudas, B., Effect of inlet turbulence on compressible flow through the tip-section turbine blade cascade with supersonic inlet, MATEC Web of Conferences 168, 2018. <https://doi.org/10.1051/mateconf/201816802007>

- [11] Synáč, J., Rudas, B., Luxa, M., Fürst, J., Nominal regimes of supersonic profile cascade, AIP Conference Proceedings 2118 (2019). <https://doi.org/10.1063/1.5114772>
- [12] Szwaba, R., Kaczynski, P., Doerffer, P., Roughness effect on shock wave boundary layer interaction area in compressor fan blades passage, Aerospace Science and Technology 85 (2019) 171–179. <https://doi.org/10.1016/j.ast.2018.12.006>